Heterogeneous CO_2 Evolution from Oxidation of Aromatic Carbon-Based Materials

Juan F. Orrego,[†] Felipe Zapata,[†] Thanh N. Truong,*[,‡] and Fanor Mondragón*[,†]

Institute of Chemistry, University of Antioquia, Medellín, Colombia, and Henry Eyring Center for Theoretical Chemistry, Department of Chemistry, University of Utah, 315 South 1400 East, Room 2020, Salt Lake City, Utah 84112

Received: April 11, 2009; Revised Manuscript Received: May 25, 2009

Carbon dioxide is one of the main gaseous products in oxidation of carbonaceous materials via both homogeneous and heterogeneous reactions. However, the mechanisms of heterogeneous CO_2 evolution during oxidation of aromatic carbon-based materials are not known in detail. Using density functional theory, a new oxidation mechanism of aromatic hydrocarbons with atomic oxygen was suggested to consist of four main steps, namely, (1) adsorption of oxygen atom, (2) insertion of O atom into the ring, (3) rearrangement to form a five-membered ring and four-membered ring lactone group, and (4) desorption of CO_2. Using naphthoxy radical as a model system, the proposed reaction pathway can explain how some of the experimentally observed CO_2 is formed.

Introduction

Oxidation of aromatic carbon-based materials is an important reaction in gasification of biomass and coal, in soot formation, and in combustion of hydrocarbon fuels. To improve efficiencies and to lower the environmental impact of these processes, it is necessary to have better knowledge of the mechanisms of this oxidation reaction. It has been accepted that the first step in oxidation of carbonaceous material is the chemisorption of oxygen on the surfaces of pores and the formation of carbon−oxygen (C(O)) complexes.[1] This is often represented by the reaction $C_f + O_2 \rightarrow 2C(O)$, where C_f is an active site. The following steps can include the decomposition of these complexes to gaseous products and the generation of new active sites for the oxidation reactions.[1,2] The oxygen-containing complexes are located mainly at defects or at edge-atom sites of the carbonaceous material.[3−5] These complexes can undergo different reactions such as rearrangements and surface migrations before they are desorbed as CO.[6] Simulation of the combustion reactions has been usually undertaken considering a char particle where the following heterogeneous reactions take place:[7,8] $C_{(s)} + O_2 \rightarrow CO_2$, $C_{(s)} + CO_2 \rightarrow 2CO$, $C_{(s)} + {}^1/_2O_2 \rightarrow CO$. Once the CO is desorbed the homogeneous reaction $CO + {}^1/_2O_2 \rightarrow CO_2$ can take place. However, the predicted concentration of CO_2 is usually lower than the experimental one,[7] which suggests other sources contributing to the production of CO_2. Additionally, the above description does not provide enough insight at a molecular level of the elementary reactions and of the complete oxidation process.

The nature of the oxygen−carbon complexes has been investigated using several experimental techniques. One of the most common is temperature-programmed desorption (TPD),[9−12] in which the functional groups are assessed through their decomposition products. However, difficulties in the interpretation of the TPD profiles may arise due to secondary reactions.[13] In general, CO_2 desorption has been suggested to be originated from carboxilate groups,[9,12] carbonate groups,[12,14] and lactones.[9,10] Decompositions between 600 and 950 K have been tentatively assigned to carboxylic anhydride or to lactones because they are more stable than the carboxylic group. However, very little information has been published for complexes decomposing into CO_2 at higher temperatures.[9] It has been published that migrations of oxygen complexes during char combustion may play an important role in the increasing of the overall CO_2 formation at high temperatures ($T \geq 1000$ K).[1]

Detailed study on mechanisms of oxidation of carbonaceous materials experimentally is difficult due to a large number of reactions taking place in the gas phase and at the solid−gas interface. Computational chemistry calculations have been carried out by different authors to characterize carbon oxygen complexes to help interpret the experimental results.[15−18] Yang et al.[15] proposed that the presence of an epoxy complex close to an edge semiquinone group in a graphene layer weakens the C−C bonding neighbor to the semiquinone group by about 33%. This suggests that the epoxy group facilitates the release of a CO molecule. Li et al.[16] have also provided insight into the atomic level mechanisms of graphite oxidation using the DFT approach. They suggested that the epoxy groups tend to line up on the graphite surface to act cooperatively pushing apart and stretching the C−C bond, breaking up the atomic structure of graphite.[3,16] Sánchez et al.,[17] using quantum chemistry methods, have demonstrated that carbon oxidation reactions in the presence of epoxy functionalities are very important in the formation of heterogeneous CO_2 and of cyclic ether complexes. Additionally, heterogeneous CO_2 evolution can be generated as a secondary reaction from a carbonate group formed by CO readsorption.[17,18]

Atomic oxygen is more reactive than molecular oxygen for the graphene oxidation, as shown by Paredes et al.,[19] using scanning tunneling microscopy (STM) and atomic force microscopy (AFM). Atomic oxygen was suggested to react not only with carbon atoms at defects but also with those located at basal planes. This explains the disappearance of the atomically flat terraces and the appearance of a generally roughened

* Corresponding authors. F.M.: E-mail, fmondra@quimbaya.udea.edu.co; fax, +574 219 6565; tel, +574 219 66 14. T.N.T: E-mail, Thanh.Truong@utah.edu.

[†] University of Antioquia. E-mail: J.F.O., jforrego@gmail.com; F.Z., tifonzafel@gmail.com.

[‡] University of Utah.

10.1021/jp903362g CCC: $40.75 © 2009 American Chemical Society
Published on Web 07/01/2009

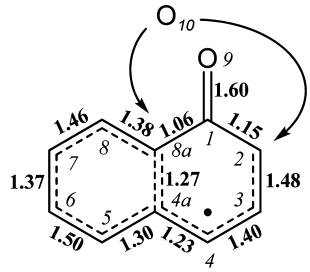

A0 Naphthoxy radical (0.0)

Figure 1. 1-Naphthoxy radical with the nomenclature used in the present research and the corresponding Wiberg's bond orders.

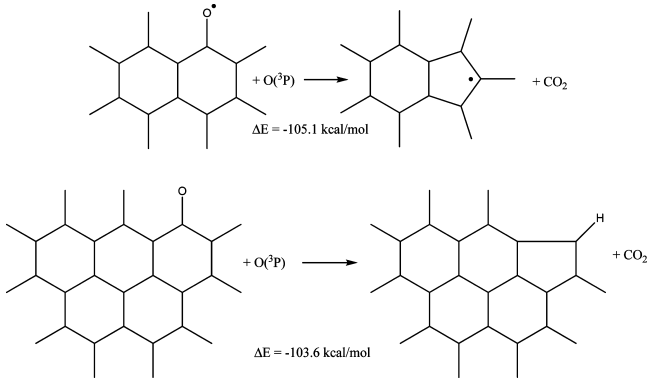

Figure 2. Relative energy of the heterogeneous CO_2 release from naphthoxy radical and an oxidized five six-membered rings of carbon at B3LYP/6-31G(d) level of theory.

topography on the samples. Nonetheless, the formation mechanism of CO and CO_2 was not discussed in such study.

It is known that concentration of atomic oxygen $O(^3P)$ in combustion systems at high temperatures (above about 1100 K) is noticeable. It can be produced through the reaction of a hydrogen atom with molecular oxygen via $^{\bullet}H + O_2 \rightarrow O(^3P) + {}^{\bullet}OH$, which consumes one radical and produces two new O and $^{\bullet}OH$ radicals becoming the most dominant chain branching reaction.[20,21] These oxygen atoms are reactive and can attack the carbonaceous framework in different positions.[22] In this work, quantum mechanic calculations have been carried out to investigate a new mechanism for oxidation carbonaceous materials for the production of heterogeneous CO_2 through the reaction with an oxygen atom in triplet state, $O(^3P)$. The mechanism includes four main steps: (1) $O(^3P)$-addition to the basal plane carbon atom adjacent to a semiquinone >C═O group (note that oxygen atom can also adsorb on the graphene layer at other locations and then migrates to the carbon atom adjacent to the semiquinone group); (2) insertion of this oxygen atom into the six-membered ring to form a seven-membered ring; (3) rearrangement of the seven-membered ring to five-membered ring and four-membered ring lactone group; (4) desorption of CO_2. Independently from our work, Radovic recently suggested the possibility of such a pathway;[23] however, no evidence was provided and no information on how the initial oxygenated species are formed.

Methodology

Geometries and frequencies of equilibrium and transition state structures were calculated using a density functional theory (DFT)[24] hybrid functional B3LYP[25,26] with the 6-31+G(d), 6-311G(d,p), and 6-311G++(d,p) basis sets to evaluate their effects on the barrier heights at the B3LYP level of theory. The B3LYP method is known to give rather accurate reaction energies, geometries, and vibrational frequencies of aromatics hydrocarbons and their radicals.[27,28] However, B3LYP has been known to underestimate the reaction activation energies for a number of reactions.[29] Single-point energy calculations at the QCISD(T)/6-31G(d)//B3LYP/6-31G(d) and QCISD(T)/6-31G(d)//B3LYP/6-31+G(d) levels were also performed to improve the energetic data. The QCISD(T)/6-31G*//B3LYP/6-31G* approach was suggested by Bach et al.,[30] in studying epoxidation reactions, where the activation barriers calculated at the QCISD(T)/6-31G*//B3LYP/6-31G* level are close to those computed at the more sophisticated QCISD(T)/6-31G*. Natural bond orbital (NBO)[31] analysis were performed and bond orders are represented by the Wiberg index.[32] For the discussion below, notation of **A** and **TS** are used for a minimum and transition state on the potential energy surface, respectively. Unless otherwise specified, QCISD(T)/6-31G(d)//B3LYP/6-31+G(d)

TABLE 1: Relative Energies (kcal/mol) Calculated at Different Levels of Theory

	B3LYP					
	6-31+G(d)	6-311G(d,p)	6-311++G(d,p)	QCISD(T)//B3LYP[a]	QCISD(T)//B3LYP[b]	PG, ES, N_{imag}[c]
A0	0.0	0.0	0.0	0.0	0.0	C_s, ^{2}A, 0
A1	−38.6	−38.0	−37.6	−41.3	−41.9	C_1, ^{2}A,0
TS1	−26.6	−25.7	−26.0	−23.3	−23.7	C_1, ^{2}A, 1
A2	−28.8	−28.9	−28.9	−28.6	−30.4	C_1, ^{2}A, 0
TS2	−26.7	−27.7	−27.8	−24.4	−24.7	C_1, ^{2}A, 1
A3	−85.9	−86.9	−85.4	−77.7	−78.3	C_s, ^{2}A", 0
TS3	−43.6	−44.5	−43.7	−43.0	−43.5	C_1, ^{2}A, 1
A4	−61.0	−61.1	−60.7	−63.3	−63.8	C_1, ^{2}A, 0
TS4	−59.9	−59.9	−59.7	−59.1	−59.9	C_1, ^{2}A, 1
A5	−69.0		−69.2		−66.9	C_1, ^{2}A, 0
TS5	−68.4		−68.6		−62.4	C_1, ^{2}A, 1
A6	−103.6	−109.0	−107.8	−102.5	−103.0	C_{2v}, $^2A_2$, 0
A7	−58.2	−58.3	−58.1	−57.0	−57.4	C_1, ^{2}A,0
TS6	−48.4	−48.4	−47.9	−47.0	−42.7	C_1, ^{2}A, 1
A8	−83.2	−84.8	−82.8	−76.8	−77.3	C_s, ^{2}A″, 0
TS7	−42.6	−43.5	−42.6	−42.3	−42.8	C_1, ^{2}A, 1
A9	−57.9	−58.4	−57.7	−60.6	−61.2	C_1, ^{2}A, 0
TS8	−45.8	−46.8	−46.5	−41.2	−41.6	C_1, ^{2}A, 1

[a] Using the QCISD(T)/6-31G(d)//B3LYP/6-31G(d) approach. [b] Using the QCISD(T)/6-31G(d)//B3LYP/6-31+G(d) approach. [c] For **A0** data of point group, PG, electronic state, ES, and number of imaginary frequencies, N_{imag}, are to naphthoxy radical, and in **A6** data are to indenyl radical.

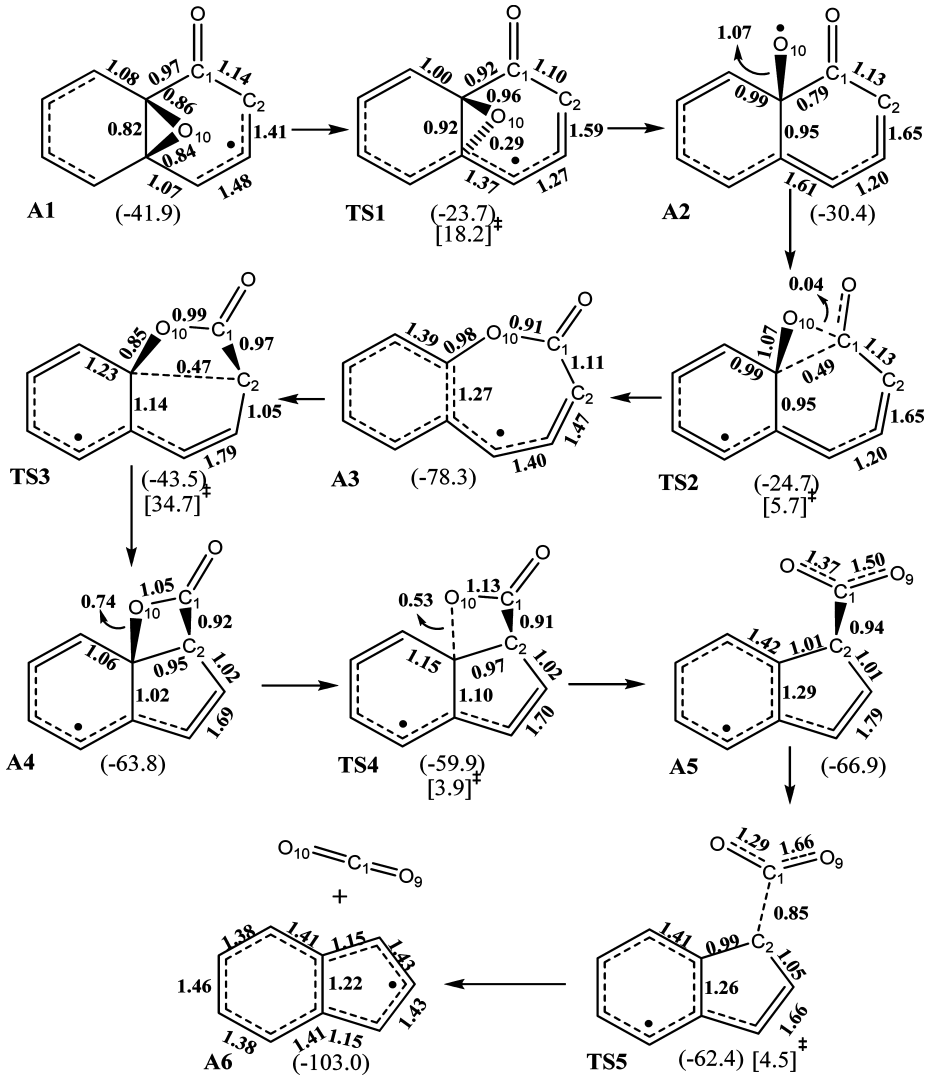

Figure 3. Reaction pathway I of heterogeneous CO_2 evolution through 1-benzoxepinyl formation. Wiberg bond orders which present a larger change are also shown. In parentheses is the energy value relative to naphthoxy radical in kcal/mol using the QCISD(T)/6-31G(d)//B3LYP/6-31+G(d) approach. In brackets is the relative value of the classical barrier for each step (Table 2).

energy values are used in the following discussion. Stable products and transition states were verified by normal-mode analyses. Specifically, minima on the potential energy surface (PES) were confirmed to have all real vibrational frequencies. For the transition state, the eigenvector of the only one imaginary frequency corresponds to the motion of the reaction coordinate. Intrinsic reaction coordinate (IRC)[33] calculations were performed at each transition state to confirm the corresponding reactants and products. All calculations were done using the Gaussian 03 package.[34]

Results and Discussion

The naphthoxy radical, shown in Figure 1 with its corresponding numbering of atoms and the Wiberg index for each bond, was used as a physical molecular model in this study. This model was selected by relying on the findings of Montoya et al.,[35] where it was shown that the CO_2 adsorption energy strongly depends on the nature of the local active site rather than on the size of the molecular model. The size-independent reactivity of the edges of the carbon model was also confirmed with the results of this research. For example, a difference of about 1.5 kcal/mol in the desorption of CO_2 from the naphthoxy structure and from an oxidized graphene layer of five six-member rings,[35,36] shown in Figure 2, confirms such a finding and supports the choice of the model.

It is possible that the size dependence is more noticeable at the transition states. The small size of the naphthoxy radical facilitates a more thorough search of the potential energy surface for paths leading to CO_2 production. The naphthoxy radical, which has a semiquinone group, has been proposed as one of the main intermediates in the naphthalene oxidation at high temperatures.[37,38] This radical can be formed by different routes. One of them is the $O(^3P)$-addition reaction to the carbon C_1 in naphthalene, which is the most reactive position in naphthalene,[39] followed by hydrogen elimination. Another possibility is the formation of the 1-naphthyl radical by hydrogen abstraction from naphthalene by the OH radical and then combining with one of the radicals O, O_2, or HO_2.[37,38]

Once the naphthoxy radical is formed, two possible reaction pathways can be considered for the heterogeneous CO_2 evolution, resulting from two possible adsorption carbon sites next to the semiquinone group. Note that CO evolution is also possible from the naphthoxy radical as shown by Kunioshi at al.[40] and from larger carbonaceous models.[41,42]

Table 1 lists relative energies calculated at different levels of theory and basis sets. It can be seen that the basis sets have

TABLE 2: Classical Barrier Heights (kcal/mol) Calculated at Different Levels of Theory

	B3LYP				
step	6-31+G(d)	6-311G(d,p)	6-311++G(d,p)	QCISD(T)//B3LYP[a]	QCISD(T)//B3LYP[b]
A1 → TS1	12.0	12.3	11.6	18.0	18.2
A2 → TS2	2.0	1.2	1.1	4.2	5.7
A3 → TS3	42.2	42.4	41.7	34.7	34.7
A4 → TS4	1.1	1.2	1.0	4.2	3.9
A5 → TS5	0.6		0.6		4.5
A7 → TS6	9.7	9.9	10.2	10.0	14.7
A8 → TS7	40.5	41.3	40.2	34.5	34.6
A9 → TS8	12.1	11.6	11.2	19.4	19.6

[a] Using the QCISD(T)/6-31G(d)//B3LYP/6-31G(d) approach. [b] Using the QCISD(T)/6-31G(d)//B3LYP/6-31+G(d) approach.

little effect on the relative reaction energies and barrier heights at the B3LYP level. At this theory level it was not possible to determine the geometries of **A5** and **TS5** using the basis set 6-31G(d) and 6-311G(d,p). Therefore, the QCISD(T)/6-31G(d)//B3LYP/6-31+G(d) approach was used to compensate the deficiencies found with the 6-31G(d) basis. Energy values agree closely with those calculated at QCISD(T)/6-31G(d)//B3LYP/6-31G(d) in almost all cases.

There are two possible pathways for addition of an O(^{3}P) atom to an adjacent carbon atom to the C═O group of the naphthoxy radical. Pathway I is shown in Figure 3. In this pathway, an O(^{3}P) atom chemisorbs on the basal plane to form an out-of-plane epoxy group at the $C_{4a}-C_{8a}$ bond (**A1** structure in Figure 3). Note that C_{4a} and C_{8a} are among those (C_2, C_4, C_5, C_7, and C_{8a}) that have the largest Mulliken atomic spin densities and thus are more susceptible to be attacked by the O(^{3}P) atom. The formation of the epoxy, **A1**, is exothermic by 41.9 kcal/mol (see Table 1), despite the fact that the aromaticity of the structure is disrupted due to the new sp^3 hybridization of C_{4a} and C_{8a}. Once **A1** is produced, the epoxy group can undergo migration, in which a stable intermediate **A2** is formed with relative energy of −30.4 kcal/mol (relative to the starting separated reactants) via the barrier **TS1** of 18.2 kcal/mol (Table 2).

In a recent study, Li et al.,[16] using $C_{54}H_{18}$ as molecular model of a graphene layer, reported a relative energy barrier of ∼20.8 kcal/mol for the similar migration of an epoxy group on the basal plane. The differences between our data and that of Li et al.[16] can be attributed to the fact that the **A1** and **TS1** structures have an unpaired electron, which can facilitate the cleavage of the $C_{4a}-O_{10}$ bond to produce the **A2** structure. The bond order of $C_{4a}-O_{10}$ in **TS1** is 0.29, supports this argument. Note that **A2** is 11.5 kcal/mol less stable compared to **A1** and is readily transformed into a more stable intermediate **A3** by insertion of the epoxy oxygen atom into the ring to form a seven-member ring lactone group, 1-benzoxepinyl, via the transition state **TS2**, as shown in Figure 3. The barrier for this process is only 5.7 kcal/mol. The Wiber index in **TS2** shows that $O_{10}-C_1$ bond order is just 0.04. The IRC calculation for **TS2** (see Figure 4) reveals the two-stage mechanism for this insertion. First the $C_{8a}-C_1$ bond is broken before the $O_{10}-C_1$ bond (ring formation) can be occur. The **A3** formation has an exothermicity of 78.3 kcal/mol (see Table 1).

The subsequent step is the reorganization of the seven member ring containing the lactone group into a five-member ring stable intermediate **A4** where the new $C_{8a}-C_2$ bond is formed. It has a barrier of 34.7 kcal/mol and is the limiting step in the whole pathway. The final step is the CO_2 elimination through a stepwise process. First, the $C_{8a}-O_{10}$ bond of the **A4** structure cleavages because it has smaller bond order of 0.74 compared to 0.92 of the C_1-C_2 bond. The step requires just

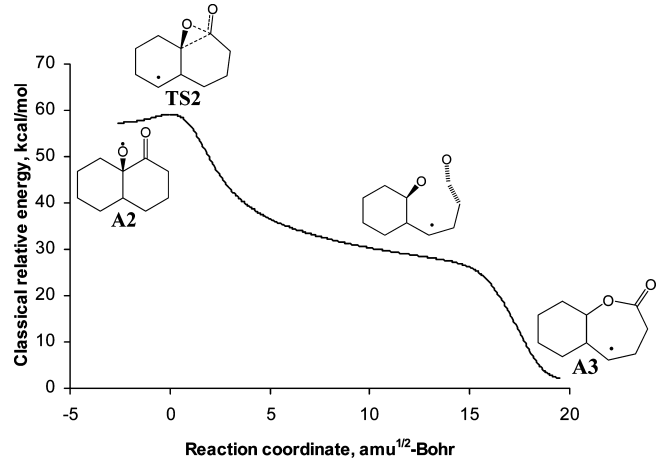

Figure 4. Intrinsic reaction coordinate (IRC) of the **TS2** structural transformation into **A3** (1-benzoxepinyl).

3.9 kcal/mol. The following step is the C_1-C_2 bond elimination to release CO_2 and an indenyl radical A6. The indenyl radical has a significant resonance stabilization energy which has been observed to form in naphthalene oxidation systems.[38]

The other possible pathway (pathway II) for addition of O(^{3}P) atom to the naphthoxy structure is at the C_2 atom as shown in Figure 5. The O-addition to the carbon C_2 occurs without any barrier to form **A7** with an exothermicity of 57.4 kcal/mol. Similar to pathway I, the following step is the insertion of the chemisorbed oxygen atom into the ring. This step proceeds with the migration of the oxygen O_{10} toward the C_1 atom which faces an energy barrier of 14.7 kcal/mol (**A7 → TS6**) to form the new bond C_1-O_{10} while the C_1-C_2 bond is elongated (bond order of 0.63 at **TS6**) in a concerted motion. The seven member ring, **A8** (2-benzoxepinyl radical), is formed with a reaction energy of −77.3 kcal/mol. **A8** undergoes rearrangement to form **A9** with a barrier of 34.6 kcal/mol (**A8 → TS7**). The formation of the indenyl radical accompanied by the release of a CO_2 molecule requires 19.6 kcal/mol to overcome the **TS8** barrier. The formation of CO_2 takes place in a concerted process where both the $C_{8a}-C_1$ and C_2-O_{10} bonds are broken to release CO_2. This is slightly different from pathway I. However, the concerted or stepwise mechanism for the CO_2 elimination could be sensitive to the level of theory being employed. Since it is not the rate limiting step, it is not critical to the results of this study.

Figure 6 shows the schematic energy diagram of the two pathways. Since both pathways are exothermic with all transition states below the starting separated reactants, they are both important. The O(^{3}P)-addition to the carbon atom C_2 is more favorable than the epoxy group formation, it is possible that the 2-benzoxepinyl pathway (pathway II) is dominant in the high pressure limit.

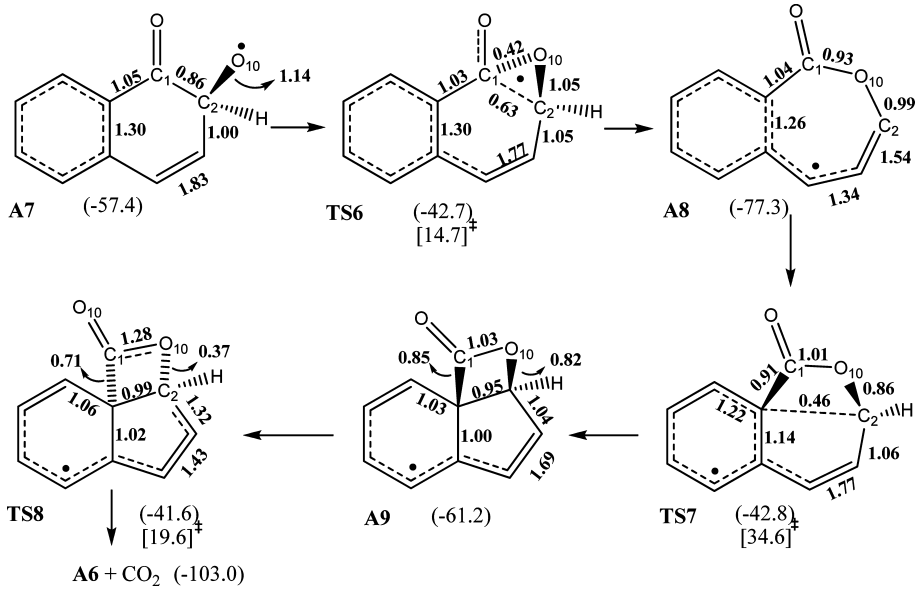

Figure 5. Reaction pathway II of heterogeneous CO_2 evolution through 2-benzoxepinyl formation. Wiberg bond orders which present a larger change are also shown. In parentheses is the energy value relative to naphthoxy radical in kcal/mol using the QCISD(T)/6-31G(d)//B3LYP/6-31+G(d) approach. In brackets is the relative value of the classical barrier for each step (Table 2).

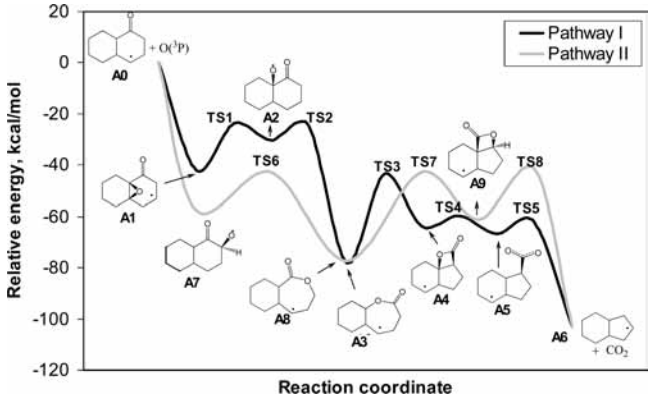

Figure 6. Comparative energy diagrams for pathway I and II of Figure 3 and Figure 6.

The above results suggest that the high temperature oxidation of carbonaceous material containing polyaromatic hydrocarbons would also take place through pathways I and II. Such a possibility is currently being investigated and will be published elsewhere. As mentioned earlier, the present results also suggest that at high temperatures the epoxy group can undergo hopping over the basal plane[22] toward the edge of the aromatic structure to a site near of a semiquinone group before CO_2 is eliminated through the present proposed mechanism. Some studies have demonstrated the significance of oxygen migration during char oxidation and its effect on CO_2 formation as well as on the bimodal nature of the CO_2 evolution profiles in TPD experiments.[1,9] Recent experiments also suggest that complexes mechanisms are involved in the CO and CO_2 evolution.[22]

The limiting step in both pathways I and II is the four-membered lactone group formation from the seven-membered lactones 1- and 2-benxozepinyl caused by thermal vibrations. That energy can be taken approximately equal to the activation energy of CO_2 desorption, E_d, corresponding to 34.5 and 34.7 kcal/mol. In an attempt to identify the functional groups corresponding to the CO_2 desorption step in TPD experiments of carbonaceous materials, Haydar et al.[9] have tentatively assigned to the CO_2 formation from carboxylic anhydride or lactone groups to the TPD signals between 600 and 950 K. These authors reported an E_d for this step between 41 and 65 kcal/mol.[9] Our results are slightly below this range but are within the uncertainty of the experimental measurements and calculations due to the different oxygenated species that could contribute to CO_2 desorption.

Concluding Remarks

Heterogeneous CO_2 evolution in oxidation of aromatic carbon-based compounds with atomic oxygen is a thermodynamically favorable reaction.

A new oxidation mechanism is proposed that is composed of four main steps: (1) atomic oxygen addition to a basal plane carbon atom adjacent to a CO group; (2) insertion of this oxygen atom into the six-membered ring to form a seven-membered ring; (3) rearrangement of the seven-membered ring into a five-membered ring and a four-membered ring lactone group; (4) CO_2 desorption.

These pathways can explain CO_2 evolution that is experimentally observed in combustion experiments and that was not able to account for by assuming only CO_2 production from gas phase homogeneous reactions.

Acknowledgment. We thank the University of Antioquia for the support of the "Sustainability Program" and the "Young Researchers Program". J.F.O. thanks "COLCIENCIAS" and the University of Antioquia for the Ph.D. scholarship.

Supporting Information Available: Tables 1S and 2S of bond lengths in Angstroms (Å) for stable species and transition states in pathway I and pathway II, respectively. Table 2S shows a comparison with others studies of bond lengths (Å) for some stable species. This material is available free of charge via the Internet at http://pubs.acs.org.

References and Notes

(1) Campbell, P. A.; Mitchell, R. E. *Combust. Flame* **2008**, *154*, 47–66.

(2) Wang, H.; Dlugogorski, B. Z.; Kennedy, E. M. *Combust. Flame* **2003**, *134*, 107–117.

(3) Ajayan, P. M.; Yakobson, B. I. *Nature* **2006**, *441*, 818–819.

(4) Radovic, L. R. *Carbon* **2005**, *43*, 907–915.

(5) Radovic, L. R.; Bockrath, B. *J. Am. Chem. Soc.* **2005**, *127*, 5917–5927.

(6) Sendt, K.; Haynes, B. S. *Proc. Combust. Inst.* **2005**, *30*, 2141–2149.

(7) Zajdík, R.; Jelemenský, L.; Remiarová, B.; Markos, J. *Chem. Eng. Sci.* **2001**, *56*, 1355–1361.

(8) Galgano, A.; Blasi, C. D.; Horvat, A.; Sinai, Y. *Energy Fuels* **2006**, *20*, 2223–2232.

(9) Haydar, S.; Moreno-Castilla, C.; Ferro-García, M. A.; Carrasco-Marín, F.; Rivera-Utrilla, J.; Perrard, A.; Joly, J. P. *Carbon* **2000**, *38*, 1297–1308.

(10) Marchon, B.; Carrazza, J.; Heinemann, H.; Somorjai, A. *Carbon* **1988**, *26*, 507–514.

(11) Hall, P. J.; Calo, J. M. *Energy Fuels* **1989**, *3*, 370–376.

(12) Boehm, H. P. *Carbon* **2002**, *40*, 145–149.

(13) Zhuang, Q.; Kyotani, T.; Tomita, A. *Energy Fuels* **1995**, *9*, 630.

(14) Kelemen, S. R.; Freund, H. *Energy Fuels* **1988**, *2*, 111.

(15) Chen, N.; Yang, R. T. *J. Phys. Chem. A* **1998**, *102*, 6348–6356.

(16) Li, J.-L.; Kudin, K. N.; McAllister, M. J.; Prud'homme, R. K.; Aksay, I. A.; Car, R. *Phys. Rev. Lett.* **2006**, *96*, 176101(1−4).

(17) Sánchez, A.; Mondragón, F. *J. Phys. Chem. C* **2007**, *111*, 612–617.

(18) Espinal, J. F.; Montoya, A.; Mondragon, F.; Truong, T. N. *J. Phys. Chem. B* **2004**, *108*, 1003–1008.

(19) Paredes, J. I.; Martínez-Alonso, A.; Tascón, J. M. D. *Carbon* **2000**, *38*, 1183–1197.

(20) Westbrook, C. K.; Mizobuchi, Y.; Poinsot, T. J. *Proc. Combust. Inst.* **2005**, *30*, 125–157.

(21) Miller, J. A.; Pilling, M. J.; Troe, J. *Proc. Combust. Inst.* **2005**, *30*, 43–88.

(22) Paci, J. T.; Upadhyaya, H. P.; Zhang, J.; Schatz, G. C.; Minton, T. K. *J. Phys. Chem. A* **2009**, *113*, 4677–4685.

(23) Radovic, L. R. Physico-Chemical Properties of Carbon Materials: a Brief Overview. In *Carbon Materials for Catalysis*; Serp, P., Figueiredo, J. L., Eds.; John Wiley & Sons: Hoboken, NJ, 2009.

(24) Parr, R. G.; Yang, W. *Density-Functional Theory of Atoms and Molecules*; Oxford Science Publications, Oxford University Press: New York, 1989.

(25) Lee, C.; Yang, W.; Parr, R. G. *Phys. Rev. B* **1988**, *37*, 785–789.

(26) Becke, A. D. *J. Chem. Phys.* **1993**, *98*, 1372–1377.

(27) Barckholtz, C.; Barckholtz, T. A.; Hadad, C. M. *J. Am. Chem. Soc.* **1999**, *121*, 491–500.

(28) Fadden, M. J.; Hadad, C. M. *J. Phys. Chem. A* **2000**, *104*, 8121–8130.

(29) Barckholtz, C.; Barckholtz, T. A.; Hadad, C. M. *J. Phys. Chem. A* **2001**, *105*, 140–152.

(30) Bach, R. D.; Glukhovtsev, M. N.; Gonzalez, C.; Marquez, M.; Estévez, C. M.; Baboul, A. G.; Schlegel, H. B. *J. Phys. Chem. A* **1997**, *101*, 6092–6100.

(31) Reed, A. E.; Curtiss, L. A.; Weinhold, F. *Chem. Rev.* **1988**, *88*, 899–926.

(32) Wiberg, K. B. *Tetrahedron* **1968**, *24*, 1083–1096.

(33) Gonzalez, C.; Schlegel, H. B. *J. Phys. Chem.* **1990**, *94*, 5523–5527.

(34) Frisch, M. J.; et al. *Gaussian 03*, revision B.02; Gaussian Inc.: Pittsburgh PA, 2003.

(35) Montoya, A.; Mondragón, F.; Truong, T. N. *Carbon* **2003**, *41*, 29–39.

(36) Frankcombe, T. J.; Smith, S. C. *Carbon* **2004**, *42*, 2921–2928.

(37) Shaddix, C. R.; Brezinsky, K.; Glassman, I. *Symp. (Int.) Combust. 24th* **1992**, 683–690.

(38) Brezinsky, K.; Shaddix, C. R. The Power of Analogies in Chemical Kinetics. In *Physical and Chemical Aspects of Combustion. A Tribute to Irvin Glassman*; Dryer, F. L., Sawyer, R. F., Eds.; Gordon and Breach Science: Amsterdam, 1997.

(39) Orrego, J. F.; Truong, T. N.; Mondragón, F. *J. Phys. Chem. A* **2008**, *112*, 8205–8207.

(40) Kunioshi, N.; Touda, M.; Fukutani, S. *Combust. Flame* **2002**, *128*, 292–300.

(41) Frankcombe, T. J.; Smith, S. C. *Carbon* **2004**, *42*, 2928.

(42) Montoya, A.; Truong, T.-T.; Mondragon, F.; Truong, T. N. *J. Phys. Chem. A* **2001**, *105*, 6757–6764.

JP903362G